DALTON
FULL PAPER

Crystal structures and Mössbauer spectra of mixed-valence dinuclear iron(II,III) complexes: detrapped valence states †

Teruaki Manago,[a] Shinya Hayami,[a] Hiroki Oshio,[b] Susumu Osaki,[c] Hiroki Hasuyama,[d] Rolf H. Herber[e] and Yonezo Maeda *[a]

[a] *Department of Chemistry, Faculty of Science, Kyushu University, Hakozaki, Higashi-ku, Fukuoka 812-8581, Japan. E-mail: y.maescc@mbox.nc.kyushu-u.ac.jp*
[b] *Department of Chemistry, Faculty of Science, Tohoku University, Aoba, Aramaki, Sendai 980-8578, Japan*
[c] *Radioisotope Center, Kyushu University, Hakozaki, Higashi-ku, Fukuoka 812-8581, Japan*
[d] *Kurume Institute of Technology, 2228 Kamitsu-machi, Kurume 830-0052, Japan*
[e] *Racah Institute of Physics, Givant Ram Campus, The Hebrew University of Jerusalem 91904, Jerusalem, Israel*

Received 19th October 1998, Accepted 1st February 1999

Mixed-valence μ-phenolate bis(μ-carboxylate) diiron(II,III) complexes $[Fe^{II}Fe^{III}(bpmp)(L)_2][BF_4]_2$ have been prepared, where Hbpmp represents 2,6-bis[bis(2-pyridylmethyl)aminomethyl]-4-methylphenol and HL is benzoic acid (Hba) **1**, phenylacetic acid (Hpaa) **2**, 3-phenylpropionic acid (Hppa) **3**, 4-phenylbutyric acid (Hpba) **4**, 5-phenylvaleric acid (Hpva) **5**, 6-phenylhexanoic acid (Hpha) **6** or *p*-methoxybenzoic acid (Hmba) **7**. The Mössbauer spectra were measured for the complexes and the crystal structures of **4** and **7** determined. Complexes **1**, **2** and **4** show trapped Mössbauer spectra due to iron(II) and iron(III), **5**–**7** show detrapped Mössbauer spectra at 293 K and trapped ones at 78 K and **3** shows a similar temperature dependence to that of **1**, but differs in some points. The quadrupole splittings and isomer shifts of **3** increase on rising temperature. The spectra are explained in terms of intramolecular electron exchange between two energetically inequivalent vibronic states $Fe_A^{2+}Fe_B^{3+}$ and $Fe_A^{3+}Fe_B^{2+}$: the apparent valence states of the iron atoms are 2.2 and 2.8 on the Mössbauer timescale at 293 K. At both 293 and 130 K the cations of complex **7** sit on a center of symmetry, and the two irons in this cation are crystallographically equivalent. The mean Fe–O length is intermediate between Fe^{II}–O and Fe^{III}–O values, which indicates that both iron atoms are in an averaged valence state at 293 and 130 K when considered in terms of a static description. However, Mössbauer spectra of the complex show that the valence states of the irons are localized to iron-(II) and -(III) at 130 K and are delocalized at 293K on the characteristic Mössbauer timescale. Complex **4** is composed of iron-(II) and -(III) moieties, in accordance with the observation that the valence states of the irons are localized on the Mössbauer timescale (10^{-7} s) at 293 K.

Diiron complexes with a variety of multidentate ligands have been intensively studied in recent years, since it is known that dinuclear iron clusters in the active sites of metalloproteins play an important role in biological systems such as haemerythrin,[1,2] R2 protein of ribonucleotide reductase,[3] methane monooxygenase,[4–6] and purple acid phosphatase.[7–9]

The bpmp complexes drawn in Chart 1 have a μ-phenolate bis(μ-carboxylate) diiron core similar to the active centers in the metalloproteins, and it is all the more significant, for an understanding of the intramolecular electron transfer between two iron atoms in biological systems, to know the mechanism of the temperature dependence of the electron transfer rate and what factors affect this rate. Mixed-valence dinuclear iron(II,III) complexes with a septadentate polypyridine ligand{Hbpmp = 2,6-bis[bis(2-pyridylmethyl)aminomethyl]-4-methylphenol} were synthesized by Suzuki *et al.*[10] and diiron(II,III) complexes with ligands which contain 1-methylimidazole instead of the pyridine groups,[11] or which have two phenol groups substituted for two of the pyridine groups,[12] were also reported. The goal of the investigations of the bpmp complexes is not only in studying the properties of model compounds for the biological systems in solution, but also in elucidating the valence states in the solid state, because the complexes with carboxylic acids having a long chain $CH_3(CH_2)_nCO_2H$, $n = 3$–7, show a detrapped valence state above 260 K, as has been reported by our group.[13] Biferrocene derivatives and trinuclear iron carboxylates with long alkyl substituents have been reported, and some of these show a temperature-dependent detrapped valence state.[14,15] Nakashima *et al.*[14] reported that biferrocene derivatives with a series of long alkyl chains formed a layered structure with a longer or shorter interlayer distance and that only the latter showed a detrapped valence state. These mixed-valence biferrocene derivatives and trinuclear iron carboxylates (Fe^{II}_2-Fe^{III}O complexes) have been systematically investigated by Hendrickson and co-workers[16] and Sano and co-workers[17] in connection with the mechanism of intramolecular electron transfer and the intermolecular effects on the rate of electron transfer.

Previous bpmp complexes and trinuclear iron carboxylates consist of high-spin iron-(II) and -(III), and intervalence transition (IT) bands are observed. Furthermore, dinuclear iron complexes composed of low-spin iron-(II) and -(III) have been reported by Spreer *et al.*[18] and an intense near-infrared band due to an IT is observed. In contrast, diiron complexes with a nonadentate polypyridine ligand, which has a stronger ligand field than bpmp, have been synthesized by our group[19] and indicated no observable band due to an intervalence transition between a high-spin iron(II) and a low-spin iron(III).

† *Supplementary data available*: cyclic voltammograms. Available from BLDSC (No. SUP 57497, 4 pp.). See Instructions for Authors, 1999, Issue 1 (http://www.rsc.org/dalton).

It has been reported that the motion of amino acid moieties at a rate of 10^2–10^4 s^{-1} in a region near to heme modulates the rate of electron transfer[20] and that fast photoinduced intramolecular electron transfer occurs at center-to-center separations up to 13.3 Å in a series of rigid non-conjugated bridges.[21] The discussion about how fast the reorganization of moieties in cations, anions and/or solvents associated with electron transfer in mixed valence complexes occurs is of interest. Mössbauer spectra collected for Fe_2(bimp){Hbimp = 2,6-bis[bis-(1-methylimidazol-2-ylmethyl)aminomethyl]-4-methylphenol} complexes clearly show the sensitivity of these complexes to anions, bridging ligands and solvents,[11c] and those for Fe_2-(bpmp) complexes show sensitivity to bridging ligands.[13c] The rate of electron transfer in the solid is sensitive to the packing environment because the coupling of the electronic and vibrational coordinates leads to a sensitivity to the environment.[16c,d] Kambara and Sasaki[22] have reported that the interaction between the molecular distortions in different molecules is essential to the transitions. Adachi *et al.*[23] have proposed the effect of an unusual type of quenched disorder on phase transitions for $Fe^{II}_2Fe^{III}O$ complexes.

In this paper the physical properties and structures of $[Fe_2$-(bpmp){$RC_6H_4(CH_2)_nCO_2$}$_2][BF_4]_2$ are examined to clarify the mechanism of the electron transfer.

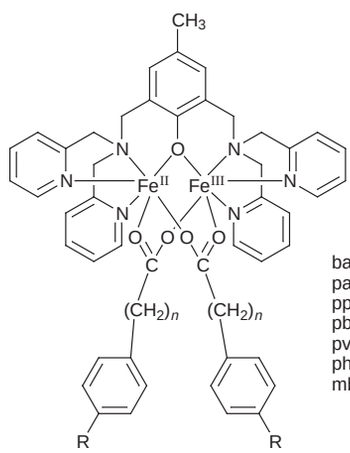

	n	R	
ba	0	H	**1**
paa	1	H	**2**
ppa	2	H	**3**
pba	3	H	**4**
pva	4	H	**5**
pha	5	H	**6**
mba	0	H	**7**
		OCH_3	

Chart 1 $[Fe_2(bpmp)(L)_2]^{2+}$.

Results and discussion

Reflectance and absorption spectra

One of the most interesting properties of transition-metal mixed-valence species is that an optical transition in the visible or near-infrared region due to intramolecular electron transitions (ITs) between different oxidation states is often observed. Reflectance and absorption spectra of the $Fe^{II}Fe^{III}$ bpmp complexes were measured in order to examine the presence of IT bands in the solid state and in acetonitrile solution, and representative spectra are shown in Fig. 1. In the reflectance spectra, a broad absorption at around 1300 nm(7690 cm^{-1}), as found previously for $[Fe^{II}Fe^{III}$(bpmp){$CH_3(CH_2)_5CO_2$}$_2][BF_4]_2$,[13] is observed, and can be assigned to IT bands. The IT bands in the reflectance spectra of **1**–**7** are nearly the same with regard to their positions, extinctions and shapes, and marked effects of the difference in carboxylic acids on the IT bands are not observed although differences in electron transfer rates are observed in the Mössbauer spectra. The IT bands in the absorption spectra for **1**–**7** are also observed in similar regions as in the reflectance spectra.

Cyclic voltammetry

Cyclic voltammograms of the complexes were measured in acetonitrile at 293 K. Two quasi-reversible waves corresponding to $Fe^{II}Fe^{II}$–$Fe^{II}Fe^{III}$, E_1, and $Fe^{II}Fe^{III}$–$Fe^{III}Fe^{III}$, E_2, couples are observed, and their potentials are collected in Table 1. The redox potentials of the complexes are dependent on the carboxylic acids, the longer the alkyl chains in $[Fe^{II}Fe^{III}$(bpmp)-{$RC_6H_4(CH_2)_nCO_2$}$_2][BF_4]_2$, the more negative are both the E_1 and E_2 values except for E_2 of **4**. The redox potentials of **7** are 42 (E_1) and 53 mV (E_2) more negative than those of **1**. From the separation of the redox potentials E_1 and E_2, comproportionation constants (K at 20 °C) of the reaction (1) were

$$(Fe^{III}–Fe^{III}) + (Fe^{II}–Fe^{II}) \rightleftharpoons 2(Fe^{III}–Fe^{II}) \quad (1)$$

calculated from (2). An increase of the separation between the

$$(E_2 - E_1) = (RT/F) \ln K \quad (2)$$

redox potentials E_1 and E_2 leads to stability of the mixed valence state. The value of the comproportionation constants increases with the length of the alkyl chain of the carboxylic acid except for **4** as shown in Table 1, then become constant above a certain length; *i.e.* the value for **6** equals that for **5**. The value for **7** is smaller than that for **1**, showing that the electron donating properties of OCH_3 on a phenyl ring bring about instability of the mixed valence state.

Table 1 Cyclic voltammetric data of the complexes

	E/V *vs.* SCE			
Complex	E_1 [a]	E_2 [b]	E_2–E_1	K [c]
1	−0.017	+0.671	0.688	6.82×10^{11}
2	−0.062	+0.644	0.706	1.39×10^{12}
3	−0.083	+0.633	0.716	2.07×10^{12}
4	−0.088	+0.638	0.726	3.07×10^{12}
5	−0.097	+0.627	0.724	2.84×10^{12}
6	−0.097	+0.627	0.724	2.84×10^{12}
7	−0.059	+0.618	0.677	4.42×10^{11}

[a] For $Fe^{II}Fe^{II}$–$Fe^{II}Fe^{III}$ redox couple. [b] For $Fe^{II}Fe^{III}$–$Fe^{III}Fe^{III}$ redox couple. [c] Comproportionation constant, E_2–$E_1 = (RT/F) \ln K$.

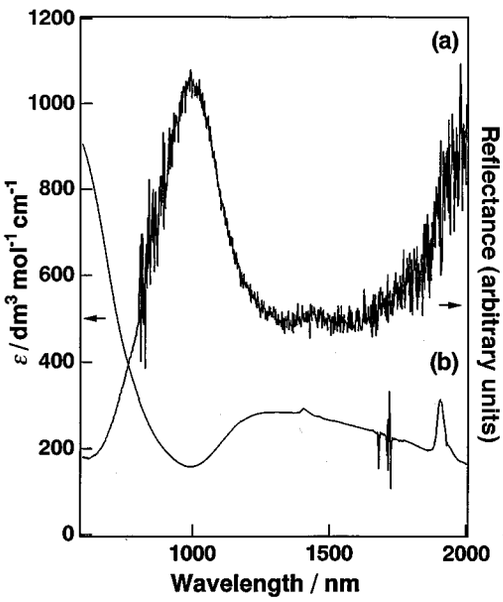

Fig. 1 (a) Reflectance spectrum of $[Fe_2(bpmp)(ppa)_2][BF_4]_2$ **3** appropriately diluted with $BaSO_4$. (b) Absorption spectrum (1×10^{-3} mol l^{-1}) in acetonitrile.

Mössbauer spectra

Mössbauer spectra of the complexes at 293 K are collected in Fig. 2. The spectra of **1**–**4** show distinct Fe^{II} and Fe^{III}, *i.e.* valence trapped, suggesting that the intramolecular electron trans-

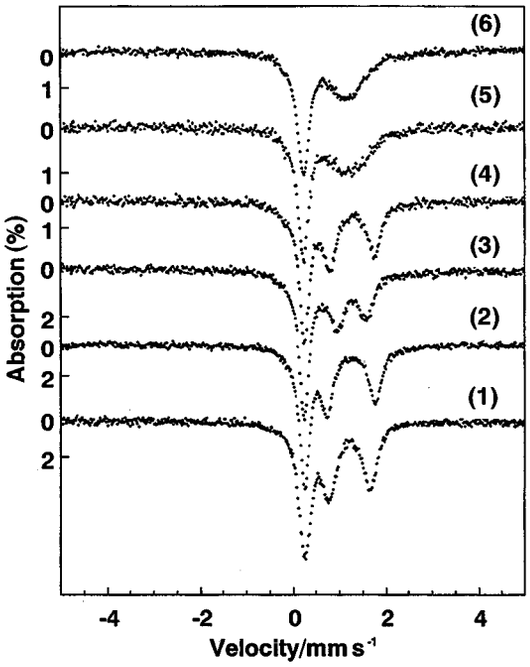

Fig. 2 Mössbauer spectra for the complexes **1**–**6** at 298 K.

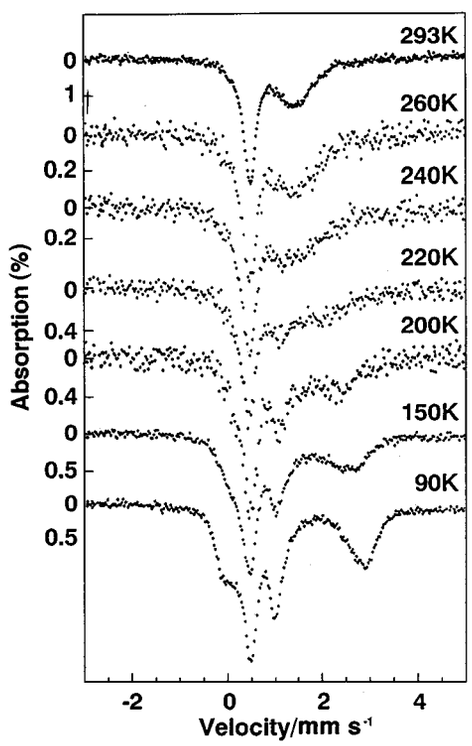

Fig. 3 Temperature dependent Mössbauer spectra for complex **6**.

fer is occurring at a rate slower than 10^6 s^{-1}. The reflectance spectra of these complexes show a band (7690 cm^{-1}) similar to the IT band observed for $[Fe^{II}Fe^{III}(bpmp)\{CH_3(CH_2)_5CO_2\}_2][BF_4]_2$,[13b] On the other hand, the Mössbauer spectra of **5** and **6** are valence detrapped at 293 K. Fig. 3 shows the spectra of **6** at various temperatures. The observed Mössbauer parameters at 90 and 293 K are listed in Table 2. The two doublets observed at 90 K gradually move together to become an apparent doublet at 293 K and line broadenings are observed. Good fits of the spectra to Lorentzian line shapes cannot be obtained in the temperature range from 150 to 260 K. The high-energy line of the doublet at 293 K is quite broad, which means that the electron transfer rate is comparable to the Mössbauer timescale or shorter. A symmetric doublet should be observed at higher

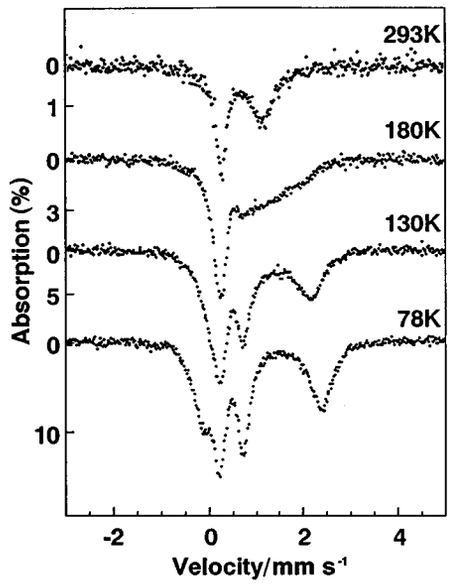

Fig. 4 Temperature dependent Mössbauer spectra for complex **7**.

temperature. The temperature at which the two doublets cannot be differentiated is *ca.* 240 K, which is close to that observed for bpmp complexes with long alkyl chains.[13a,b]

The variable temperature Mössbauer spectra of complex **7** are shown in Fig. 4 and the Mössbauer parameters at 78, 130, 293 K are collected in Table 2. Good fits of the spectra to Lorentzian line shapes cannot be obtained at 180 K because of the relaxation of the valence states. Two quadrupole-split doublets can be seen at 78 K, one characteristic of Fe^{II} with an isomer shift of 1.14 mm s^{-1} and a quadrupole splitting of 2.52 mm s^{-1}, and the other characteristic of Fe^{III} with an isomer shift of 0.47 mm s^{-1} and a quadrupole splitting of 0.52 mm s^{-1}. As the temperature is increased these two doublets gradually approach each other with line broadening to become a single average-valence doublet with an isomer shift of 0.68 mm s^{-1} (quadrupole splitting of 0.88 mm s^{-1}). The temperature at which the two kinds of doublet of **7** cannot be differentiated from each other is *ca.* 180 K, which is lower than those observed for bpmp complexes with long alkyl chains,[13a,b] the valence delocalization in **7** taking place at the lowest temperature of all of the bpmp complexes so far examined. The reflectance spectrum of **7** shows a broad IT band (7690 cm^{-1}) and the shape is very similar to that of **1**.

The electron transfer would be accompanied by a change in the arrangement of the molecules. It is said that combination of a measure of interaction between two centers and a measure of vibronic coupling is important in the PKS model.[24] If we call a domain the region where the arrangement of molecules occurs co-operatively, a small-size domain would need smaller energy for the exchange between $Fe_A^{2+}Fe_B^{3+}$ and $Fe_A^{3+}Fe_B^{2+}$ than a large-size domain.

Complex 3. The Mössbauer spectra of complexes **2** and **3** measured in the temperature range from 78 (95 for **2**) to 330 K (293 K for **2**) are illustrated in Figs. 5 and 6 respectively, and the Mössbauer parameters are collected in Table 2. The spectrum at 78 K (95 K for **2**) shows typical valence trapped doublets assigned to Fe^{II} and Fe^{III}. As the temperature is increased the two doublets approach each other, but remain even at 293 K. The temperature dependence of the spectra for **3** is apparently similar to that for **2**, but the behaviour of the isomer shifts (δ) and quadrupole splittings (ΔE) is different.

The values of the isomer shifts obtained for complexes **2** and **3** are plotted in Fig. 7 and those of the quadrupole splittings in Fig. 8. The temperature dependence of the isomer shift for **2** is normal because the differences of the values of the isomer

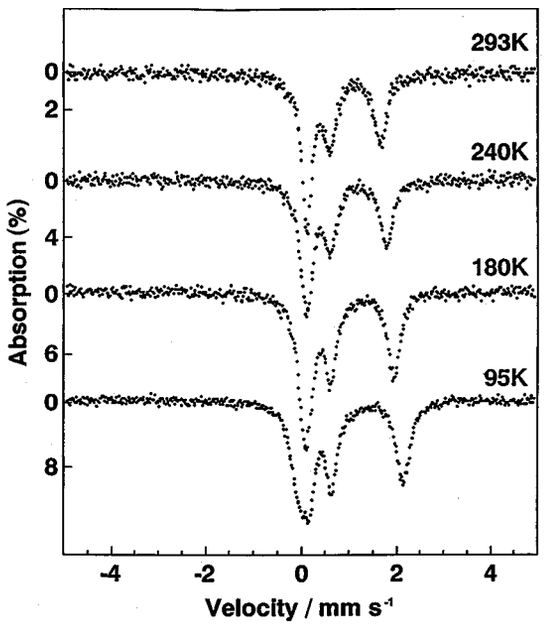

Fig. 5 Temperature dependent Mössbauer spectra for complex **2**.

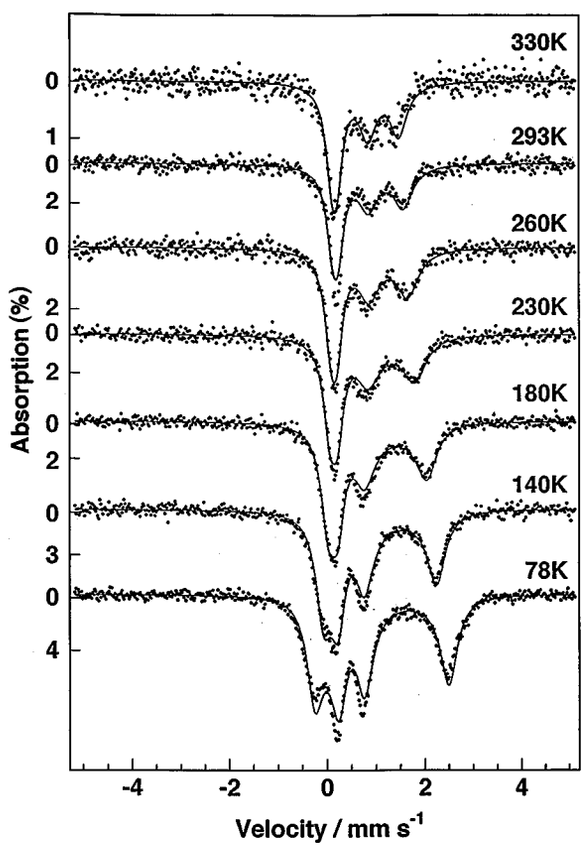

Fig. 6 Temperature dependent Mössbauer spectra for complex **3** and the fitted spectra. The parameters used for the fitting are listed in Table 3.

shifts at between 95 and 293 K are 0.17 mm s^{-1} for Fe^{II} and 0.05 mm s^{-1} for Fe^{III}, which correspond to the second order Doppler shift (usually about 0.1 mm s^{-1}).[25a] On the other hand, the isomer shift of Fe^{II} (0.844 mm s^{-1}) for **3** is slightly small for high-spin Fe^{II} at 293 K and that of Fe^{III} (0.528 mm s^{-1}) is slightly large for high-spin Fe^{III}, and the difference of the values at between 78 and 293 K are 0.256 mm s^{-1} for iron Fe^{II} and −0.058 mm s^{-1} for Fe^{III}. Furthermore, the quadrupole splitting values of Fe^{III} increase with rising temperature, which is abnormal, *i.e.* quadrupole splittings are not dependent on

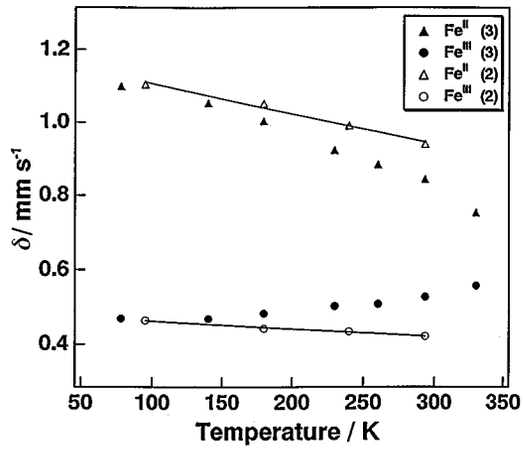

Fig. 7 Plots of the isomer shifts *vs.* temperature for complexes **2** and **3**.

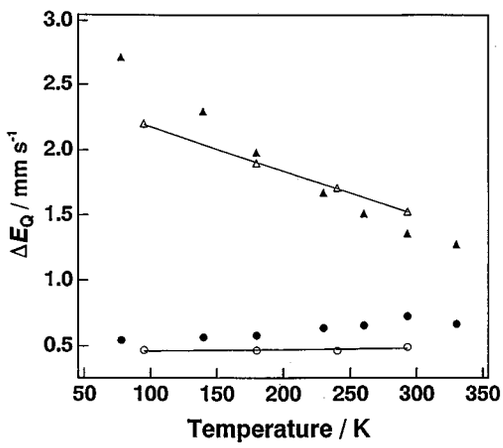

Fig. 8 Plots of the quadrupole splittings *vs.* temperature for complexes **2** and **3**. △, Fe^{II} and ○, Fe^{III} for complex **2**; ▲, Fe^{II} and ●, Fe^{III} for **3**.

temperature for high-spin iron(III) and decrease with rising temperature for high-spin iron(II) except for complexes which experience a phase transition in the measured temperature range.[26] The linewidths observed for the high-energy lines of the respective doublets for iron-(II) and -(III) of **3** show a maximum at 230 K, as listed in Table 2, which cannot be explained by spin–spin relaxation.

The isomer shift is related to the formal valence state of iron atoms.[26,27] This model assumes that typical iron-(II) and -(III) salts have $3d^64s^0$ and $3d^54s^0$ atomic configurations respectively, and a scale of the isomer shift is derived accordingly. The contribution from the outer 4s electrons is estimated by modifying the model to $3d^{n-x}4s^x$ configuration.[25b,28] Electron density at an iron nucleus is reflected in isomer shifts and the apparent valence state of an iron atom can be evaluated by the latter, if an electron is exchanged between Fe^{II} and Fe^{III} faster than the Mössbauer timescale. In fact the isomer shift of the detrapped valence state observed for $[Fe_2(bpmp)(ena)_2][BF_4]_2$ [Hena = $CH_3(CH_2)_5CO_2H$] is 0.70 mm s^{-1} at 290 K.[13b] The chemical structures for some $[Fe_2(bpmp)L_2]X_2$ have been determined and complexes with the long alkyl chain carboxylic acids have layer structures in which each iron atom is co-ordinated with three oxygen and three nitrogen atoms. The geometrical moiety and chemical bonding of iron atoms of **3** are assumed to be similar to those of **2** because the X-ray diffraction powder pattern of **3** is similar to that of **2** (described later), and therefore the isomer shifts (for localized states) of **3** would be close to those of **2**. A series of $[Fe_2(bpmp)L_2]X_2$ have similar isomer shifts to each other.[13c]

Potential energy diagrams for mixed-valence complexes are drawn for some cases in Fig. 9. In case B of Fig. 9 the Fe_A^{2+}-

Table 2 Mössbauer fitting parameters for the complexes

Complex	T/K	δ/mm s^{-1}			ΔE_Q/mm s^{-1}			Γ^a/mm s^{-1}			Area (%)		
		Fe^{II}	Fe^{av}	Fe^{III}	Fe^{II}	Fe^{av}	Fe^{III}	Fe^{II}	Fe^{av}	Fe^{III}	Fe^{II}	Fe^{av}	Fe^{III}
1	293	0.92(0)		0.48(0)	1.40(1)		0.52(1)	0.37(1)		0.38(1)	50.7(6)		49.3(5)
2	95	1.11(0)		0.47(0)	2.20(1)		0.47(1)	0.33(1)		0.29(1)	52.5(5)		47.5(6)
	180	1.05(1)		0.44(0)	1.90(1)		0.47(1)	0.30(1)		0.28(1)	50.8(6)		49.2(6)
	240	0.99(0)		0.44(0)	1.71(1)		0.47(1)	0.30(1)		0.30(1)	50.7(6)		49.3(7)
	293	0.94(1)		0.42(0)	1.53(1)		0.49(1)	0.30(1)		0.29(1)	50.2(5)		49.8(6)
3	78	1.100(2)		0.470(3)	2.718(4)		0.545(6)	0.41(1)		0.32(1)	51.8(7)		48.2(6)
								0.48(1)		0.40(1)			
	140	1.054(3)		0.469(4)	2.293(6)		0.569(9)	0.36(1)		0.31(1)	50.4(5)		49.6(6)
								0.53(1)		0.46(1)			
	180	1.004(3)		0.484(4)	1.985(7)		0.582(8)	0.35(1)		0.30(1)	49.8(7)		50.2(6)
								0.56(1)		0.54(1)			
	230	0.924(5)		0.504(6)	1.73(1)		0.64(1)	0.33(1)		0.30(1)	49.5(5)		50.5(6)
								0.58(2)		0.56(1)			
	260	0.884(5)		0.509(6)	1.617(9)		0.66(1)	0.32(1)		0.30(1)	49.0(7)		51.0(6)
								0.55(2)		0.49(2)			
	293	0.844(3)		0.528(4)	1.501(7)		0.727(8)	0.30(1)		0.30(1)	48.9(5)		51.1(6)
								0.42(2)		0.43(2)			
	330	0.75(1)		0.56(1)	1.28(2)		0.67(2)	0.30(1)		0.30(1)	48.1(7)		51.9(6)
								0.36(3)		0.50(4)			
4	78	1.14(0)		0.48(0)	2.40(1)		0.56(1)	0.38(1)		0.27(1)	51.8(7)		48.2(6)
	293	0.98(0)		0.49(0)	1.49(1)		0.55(1)	0.36(1)		0.35(1)	50.4(5)		49.6(6)
5	293		0.70(1)			1.02(2)			0.28(1)			100	
									0.98(3)				
6	90	1.12(1)		0.46(0)	2.78(1)		0.51(1)	0.53(1)		0.32(1)	51.6(9)		48.4(6)
								0.65(1)		0.33(1)			
	293		0.69(1)			1.00(2)			0.27(1)			100	
									0.83(3)				
7	78	1.14(0)		0.47(0)	2.52(1)		0.52(1)	0.45(1)		0.31(1)	51.7(9)		48.3(6)
								0.55(1)		0.33(1)			
	130	1.14(1)		0.47(0)	2.06(1)		0.55(1)	0.46(1)		0.32(1)	51.2(8)		48.8(6)
								0.73(2)		0.37(2)			
	293		0.68(1)			0.88(1)			0.27(1)			100	
									0.58(2)				

[a] Half-width at half-maximum listed in order of increasing velocity of the peak.

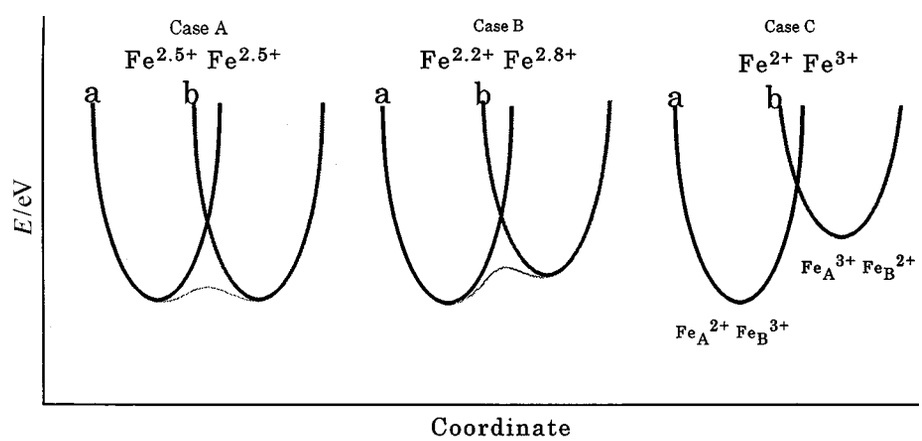

Fig. 9 Potential energy diagrams for mixed-valence dinuclear iron(II,III) complexes. Curve a is for the $Fe_A^{2+}Fe_B^{3+}$ state and b for $Fe_A^{3+}Fe_B^{2+}$. Case A: for delocalized valence states. Case B: for energetically inequivalent vibronic states. An excess electron (a valence electron of Fe^{2+}) stays 80% of the time in the $Fe_A^{2+}Fe_B^{3+}$ state and 20% in the $Fe_A^{3+}Fe_B^{2+}$ state. Case C: for localised valence states.

Fe_B^{3+} state is slightly more stable than the $Fe_A^{3+}Fe_B^{2+}$ state. The dynamic electron exchange between two energetically inequivalent sites, A and B, is considered to explain the temperature dependence of the isomer shifts and quadrupole splittings: an excess electron (an electron of Fe^{2+}) stays a little longer on the A than on the B site. It is assumed on the basis of the difference in isomer shifts of **3** from that of **2** at 293 K that an excess electron stays 80% of the time at the A site and 20% of the time at the B site. If the electron exchange rate increases from *ca.* 10^6 to *ca.* 10^8 s^{-1} with rising temperature the dynamic electronic states should be reflected in the Mössbauer spectra. The theoretical spectra for the model can be calculated by using Wickman's method;[29] the final spectrum is composed of the two relaxation spectra, iron of the A site and that of the B site.

The theoretical spectra are calculated from eqns. (1)–(8)

$$I(\bar{\omega}) = K\Sigma_i\{[1 + \tau_i\Gamma)P_i + Q_iR_i]/(P_i^2 + R_i^2)\} \quad (1)$$

$$P_1 = \tau_1[\Gamma^2 - (\Delta_1 - \bar{\omega})^2 + \delta_1^2] + \Gamma \quad (2)$$

$$Q_1 = \tau_1[\Delta_1 - \bar{\omega} - (p_{11} - p_{12})\,\delta_1] \quad (3)$$

$$R_1 = (\Delta_1 - \bar{\omega})(1 + 2\tau_1\Gamma) + (p_{11} - p_{12})\,\delta_1 \quad (4)$$

$$P_2 = \tau_2[\Gamma^2 - (\Delta_2 - \bar{\omega})^2 + \delta_2^2] + \Gamma \quad (5)$$

$$Q_2 = \tau_2[\Delta_2 - \bar{\omega} - (p_{21} - p_{22})\,\delta_2] \quad (6)$$

Table 3 Mössbauer parameters used for the theoretical fitting for complex **3**

	δ/mm s^{-1}		ΔE/mm s^{-1}				
T/K	Fe^{II}	Fe^{III}	Fe^{II}	Fe^{III}	τ_{11}[a]/10^2 ns[a]	τ_{11}*[b]/10^2 ns[b]	τ_1[c]/10^2 ns
78	1.12	0.51	2.79	0.48	18.3	4.6	3.7
140	1.07	0.51	2.38	0.47	14.4	3.6	2.9
180	1.03	0.50	2.11	0.45	9.4	2.4	1.9
230	0.97	0.49	1.92	0.43	4.4	1.11	0.89
260	0.94	0.47	1.78	0.43	3.1	0.77	0.62
293	0.92	0.46	1.67	0.41	2.3	0.58	0.46
330	0.87	0.46	1.57	0.41	2.1	0.52	0.42

[a] Lifetime of Fe^{2+} on the A site. [b] Lifetime of Fe^{3+} on the A site. [c] $\tau_1 = (\tau_{11}\tau_{11}^*)/(\tau_{11} + \tau_{11}^*)$.

$$R_2 = (\Delta_2 - \bar{\omega})(1 + 2\tau_2\Gamma) + (p_{21} - p_{22})\,\delta_2 \qquad (7)$$

$$\tau_1 = \tau_{11}\tau_{11}^*/(\tau_{11} + \tau_{11}^*),\ \tau_2 = \tau_{22}\tau_{22}^*/(\tau_{22} + \tau_{22}^*) \qquad (8)$$

where the subscript i refers two iron ($i = 1$, iron of the A site; $i = 2$, iron of the B site). The probabilities where the iron atom is in divalent and trivalent states on the A site are $p_{11} = 0.8$ and $p_{12} = 1 - p_{11}$, respectively, and those on the B site $p_{21} = 0.2$ and $p_{22} = 1 - p_{21}$, respectively. The four transitions correspond to ω_1 Fe^{2+}, $|\pm1/2\rangle_{gr} \leftrightarrow |\pm1/2\rangle_{ex}$ in the A state, ω_2 Fe^{2+}, $|\pm1/2\rangle_{gr} \leftrightarrow |\pm3/2\rangle_{ex}$ in the B state, ω_3 Fe^{3+}, $|\pm1/2\rangle_{gr} \leftrightarrow |\pm1/2\rangle_{ex}$ in the A state, and ω_4 Fe^{3+}, $|\pm1/2\rangle_{gr} \leftrightarrow |\pm3/2\rangle_{ex}$ in the B state. Parameters Δ_i and δ_i are given by eqns. (9)–(12). The

$$\Delta_1 = (\bar{\omega}_1 + \bar{\omega}_3)/2 \qquad (9)$$

$$\Delta_2 = (\bar{\omega}_2 + \bar{\omega}_4)/2 \qquad (10)$$

$$\delta_1 = (\bar{\omega}_1 - \bar{\omega}_3)/2 \qquad (11)$$

$$\delta_2 = (\bar{\omega}_2 - \bar{\omega}_4)/2 \qquad (12)$$

lifetimes τ_1 and τ_2 apply for an iron on each site and τ_1 is equal to τ_2 in the simulation. The values of the quadrupole splitting are varied by applying the parameters obtained for complex **2**. The average linewidth observed for **2**, 0.294 mm s^{-1}, is used for Γ because the spectra were not able to be fitted by using the natural linewidth 0.194 mm s^{-1}. Some of the calculated spectra are shown in Fig. 10, and the simulated spectra are shown as the solid lines in Fig. 6 for which the fitting parameters are listed in Table 3. The Mössbauer spectra for **3** are well fitted with the theoretical curves, which supports apparent valence states of iron in each state of about 2.2 and 2.8 at 293 K.

One of the important results from this simulation is that appreciable line broadening is not observed in the range of electron exchange rate from 10^6 to 10^8 s^{-1} although appreciable line broadening on rising temperature is observed for detrapped valence states.[13a,b] Masuda and Sano[30] explained the absence of line broadening in dialkylbiferrocenium triiodides by assuming only thermal population differences, where electron transfer rates must be much faster than the Mössbauer timescale in the temperature region of valence detrapping. A similar case has been observed for trinuclear iron carboxylates by Wu *et al.*[16f] They proposed a model that there are two types of domains, one of which is valence trapping "static" domains and the other is valence detrapping "dynamic" domains and that no line broadening is observed if "domain walls" are moving at a rate faster than the Mössbauer timescale and static domains increase with rising temperature. The example having asymmetric double minimums (case B in Fig. 9) could be observed here because the difference of the values of the isomer shift between iron-(II) and -(III) is large.

The values of τ_{11} and τ_{11}* are listed in Table 3; τ_{22} is equal to τ_{11} and τ_{22}* to τ_{11}*, the values obtained for τ_1 being close to 10^{-7} s. Plots of ln τ_1 *vs.* T^{-1} (Arrhenius plot) for complex **3** were obtained in the temperature region from 230 to 330 K. The activation energy E_a for the electron transfer was estimated to be *ca.* 5.5 kcal mol^{-1} in the temperature range 180–293 K, which is larger than *ca.* 1 kcal mol^{-1} evaluated for *trans*-μ-(*as*-indacene)-bis(cyclopentadienyliron) $[(C_{12}H_8)Fe^{II}Fe^{III}(C_5H_5)_2]I_3 \cdot 0.5I_2$.[31]

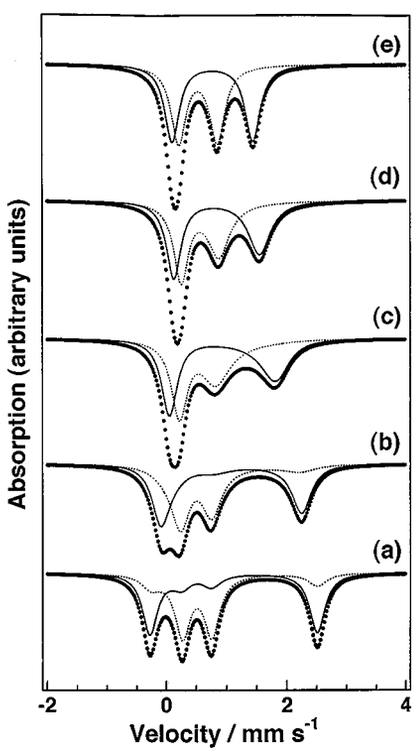

Fig. 10 Mössbauer spectra calculated from the model having two energetically inequivalent vibronic states. Mössbauer parameters for the calculation are as follows. (a) $\delta_{II} = 0.92$, $\delta_{III} = 0.44$, $\Delta E_{II} = 1.64$, $\Delta E_{III} = 0.50$ mm s^{-1}, $\tau_{11} = 100$ and τ_{11}* = 25 ns; (b) $\delta_{II} = 0.97$, $\delta_{III} = 0.45$, $\Delta E_{II} = 1.84$, $\Delta E_{III} = 0.50$ mm s^{-1}, $\tau_{11} = 200$ and τ_{11}* = 50 ns; (c) $\delta_{II} = 1.02$, $\delta_{III} = 0.46$, $\Delta E_{II} = 2.04$, $\Delta E_{III} = 0.50$ mm s^{-1}, $\tau_{11} = 300$ and τ_{11}* = 75 ns; (d) $\delta_{II} = 1.08$, $\delta_{III} = 0.47$, $\Delta E_{II} = 2.23$, $\Delta E_{III} = 0.50$ mm s^{-1}, $\tau_{11} = 500$ and τ_{11}* = 125 ns; (e) $\delta_{II} = 1.13$, $\delta_{III} = 0.48$, $\Delta E_{II} = 2.42$, $\Delta E_{III} = 0.50$ mm s^{-1}, $\tau_{11} = 800$ and τ_{11}* = 200 ns; (f) $\delta_{II} = 1.14$, $\delta_{III} = 0.49$, $\Delta E_{II} = 2.75$, $\Delta E_{III} = 0.50$ mm s^{-1}, $\tau_{11} = 1000$ and τ_{11}* = 250 ns.

Single-crystal structures of complex 7 at 293 and 130 K

Single-crystal structure determinations of complex **7** were carried out at both 293 and 130 K. An ORTEP drawing of the cation at 130 K with its atom-labeling scheme is given in Fig. 11 and selected bond distances and angles at both temperatures are listed in Table 4. Since rotational disorder of a counter anion along the F(1)–B axis of BF_4^- exists at 293 K, seven fluorine atoms were located; all fluorine atoms except F(1) were analysed with a population of 0.5. However, this disorder was not observed at 130 K. The iron atoms in the cation are bridged with a phenolate and two carboxylates, and have distorted octahedra of the N_3O_3 type. At both temperatures there is a C_2

Table 4 Selected bond lengths (Å) and angles (°) for $[Fe_2(bpmp)(mba)_2][BF_4]_2$ **7** at 130 and 293 K

	130 K	293 K
Fe–O(1)	1.992(3)	1.996(2)
Fe–O(2)	2.039(4)	2.040(3)
Fe–O(3)	1.999(4)	2.005(3)
$Fe–O_{av}$	2.010	2.014
Fe–N(1)	2.147(5)	2.145(4)
Fe–N(2)	2.191(4)	2.199(4)
Fe–N(3)	2.125(5)	2.121(3)
Fe···Fe	3.386(2)	3.395(1)
O(1)–Fe–O(2)	87.4(1)	87.5(2)
O(1)–Fe–O(3)	102.3(1)	101.4(2)
O(1)–Fe–N(1)	90.9(2)	90.7(2)
O(1)–Fe–N(2)	88.9(2)	89.4
O(1)–Fe–N(3)	161.2(1)	162.4(2)
O(2)–Fe–O(3)	95.3(2)	95.1(2)
O(2)–Fe–N(1)	170.8(2)	170.5(2)
O(2)–Fe–N(2)	92.4(2)	92.5(2)
O(2)–Fe–N(3)	81.6(2)	82.6(2)
O(3)–Fe–N(1)	93.9(2)	94.4(2)
O(3)–Fe–N(2)	166.7(2)	167.0(2)
O(3)–Fe–N(3)	93.9(2)	94.0(2)
N(1)–Fe–N(2)	78.5(2)	78.2(3)
N(1)–Fe–N(3)	97.4(2)	96.6(2)
N(2)–Fe–N(3)	76.4(2)	76.6(2)
Fe–O(1)–Fe	116.4(2)	116.9(3)

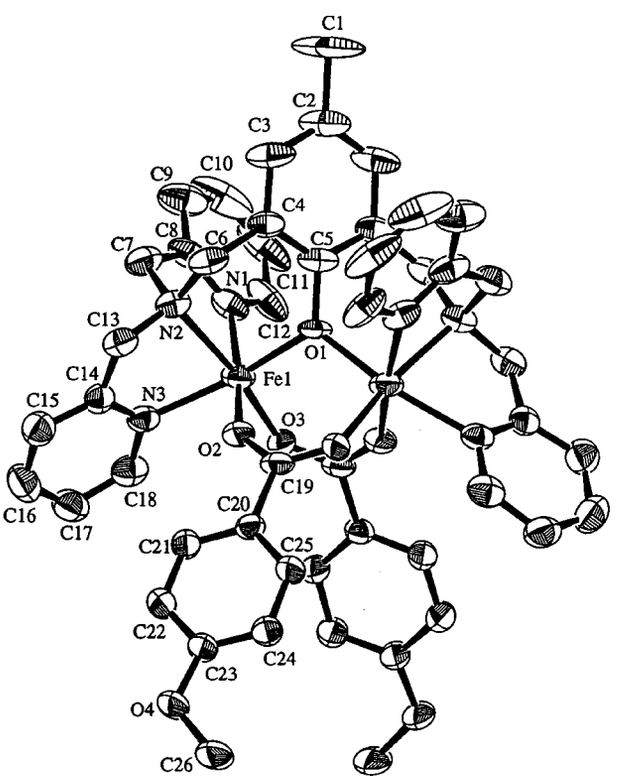

Fig. 11 Crystal structure of $[Fe_2(bpmp)(mba)_2]^{2+}$ in complex **7** at 130 K with 50% probability thermal ellipsoids.

axis in the molecule [*i.e.* C(1)–C(2)–C(5)–O(1)]. The two iron atoms are crystallographically equivalent. The average Fe–O distance is 2.014 Å at 293 K and 2.010 Å at 130 K, intermediate between Fe^{II}–O and Fe^{III}–O bond lengths. Therefore, it can be said that the two iron atoms are in an averaged valence state at 130 and 293 K. The Fe···Fe distance and the Fe–O(1)–Fe angle are 3.395(1) Å and 116.9(3)° at 293 K, and 3.386(2) Å and 116.4(2)° at 130 K, respectively. These values are comparable to those reported previously: the values found for $[Fe_2(bpmp)\{CH_3(CH_2)_5CO_2\}_2][BF_4]_2$ are 3.365(7) Å and 112.3(4)°,[13b] and those for $[Fe_2(bpmp)(CH_3CH_2CO_2)_2][BPh_4]_2$ are 3.365(1) Å and 113.1(1)°.[11d] Comparison of the refined atomic positions of the cations at 293 K with those at 130 K shows only minor shifts, none of which is significant. At first sight it seems strange that the two iron atoms are crystallographically equivalent at 130 K, although the Mössbauer spectra indicate localized trapped iron-(II) and -(III) states below 130 K. This inconsistency can be explained by the time needed for observing the Mössbauer absorption of ^{57}Fe, 10^{-7} s. The information from X-ray diffraction patterns gives an average for the range of molecules. Although trapped valence states are observed in the Mössbauer spectrum at 130 K, it does not imply that valence states are trapped on a timescale longer than 10^{-6} s.

Since the two iron moieties are equivalent at 130 and 293 K, the two vibronic states, $Fe_A^{2+}Fe_B^{3+}$ and $Fe_A^{3+}Fe_B^{2+}$, are at the same energy levels, and the potential energy barrier between them may be almost constant in the temperature range 130–293 K. Therefore, the more thermal energy the system gains, the more rapidly the intramolecular electron transfer occurs, and this transfer can be explained by an electron hopping model between iron-(II) and -(III) states. As the timescale of Mössbauer spectra is 10^{-7} s, the spectra of the complex apparently convert from those of a valence trapped to a detrapped state in the timescale range from $\approx 10^{-6}$ to $\approx 10^{-8}$ s. This process is supported by the fact that the line broadening of the spectra is peculiar to the electron hopping model.

There are some examples of structural determinations at low temperature for complexes indicating temperature-dependent valence states in biferrocene derivatives and trinuclear iron carboxylates. Recently Sato *et al.*[32] reported that the trinuclear iron chloroacetate $[Fe_3O(CH_2ClCO_2)_6(H_2O)_3]\cdot 3H_2O$ showed a valence delocalization only between two iron atoms in the crystal structure as well as in the Mössbauer spectra: structure determinations have been carried out at 112 and 293 K, which indicated that the three iron atoms were clearly assigned to an iron-(II) and two iron-(III) sites at 112 K and the iron-(II) moiety and one of the iron-(III) moieties approached each other at 293 K. The temperature dependence of the Mössbauer spectra differs from ours in that no line broadening occurs at the temperature range where the spectra changes from trapped to detrapped.

Single-crystal structure of complex 4

The crystal structure of complex **4** was determined at 293 K (Fig. 12). Selected bond distances and angles are listed in Table 5. The BF_4^- anions were found to be disordered in the same way as in **7** at 293 K, and F(2)–F(7), F(9)–F(14), of which the populations are 0.5, correspond to the two anions respectively. The cation has a distorted octahedral N_3O_3 core, being bridged with a phenolate and two carboxylates. However, no C_2 axis, like that observed in **7,** is present, and the two iron atoms in the cation are crystallographically inequivalent. As the mean Fe(1)–O and Fe(2)–O lengths are 1.966 and 2.080 Å, respectively, Fe(1) is assigned to a trivalent and Fe(2) to a divalent state. The Fe(1)···Fe(2) distance is 3.393(2) Å and the Fe(1)–O(1)–Fe(2) angle is 115.1(1)°, values similar to those observed for **7**. The conformation of the ligand bpmp in **4** is almost identical with that in **7**; however, the steric arrangements of the two carboxylic acids in **4** are not identical with each other as shown in Fig. 12.

In previous studies it has been pointed out that the onset of motions of the solvate molecules, ligands, or counter ions probably influences the rate of intramolecular electron transfer in mixed-valence trinuclear iron carboxylates and biferrocene derivatives.[33] In fact, the BF_4^- anions in **7** are converting from order to disorder in the temperature region where the Mössbauer spectra change from valence trapped to valence detrapped, and in $[Fe_2(bpmp)\{CH_3(CH_2)_5CO_2\}_2][BF_4]_2$ valence detrapped above 260 K the disorder of BF_4 anions is observed at 293 K.[13b] Disorder of the anions is also observed with **4**, exhibiting a valence trapped spectrum at 293 K. Therefore, the

Table 5 Selected bond lengths (Å) and angles (°) for $[Fe_2(bpmp)(pba)_2][BF_4]_2$ **4**

Fe(1)–O(1)	1.943(2)	Fe(2)–O(1)	2.075(2)
Fe(1)–O(2)	2.007(3)	Fe(2)–O(4)	2.036(2)
Fe(1)–O(3)	1.948(2)	Fe(2)–O(5)	2.130(3)
$Fe(1)–O_{av}$	1.966	$Fe(2)–O_{av}$	2.080
Fe(1)–N(1)	2.152(3)	Fe(2)–N(4)	2.176(3)
Fe(1)–N(2)	2.190(3)	Fe(2)–N(5)	2.195(3)
Fe(1)–N(3)	2.151(3)	Fe(2)–N(6)	2.153(3)
Fe(1)···Fe(2)	3.393(2)		
O(1)–Fe(1)–O(2)	92.16(10)	O(1)–Fe(2)–O(3)	96.36(9)
O(1)–Fe(1)–O(5)	101.97(10)	O(1)–Fe(2)–O(4)	88.83(9)
O(1)–Fe(1)–N(1)	87.9(1)	O(1)–Fe(2)–N(4)	88.3(1)
O(1)–Fe(1)–N(2)	89.98(10)	O(1)–Fe(2)–N(5)	87.48(9)
O(1)–Fe(1)–N(3)	164.6(1)	O(1)–Fe(2)–N(6)	161.8(1)
O(2)–Fe(1)–O(5)	97.1(1)	O(3)–Fe(2)–O(4)	93.7(1)
O(2)–Fe(1)–N(1)	169.7(1)	O(3)–Fe(2)–N(4)	90.7(10
O(2)–Fe(1)–N(2)	91.3(1)	O(3)–Fe(2)–N(5)	169.0(1)
O(2)–Fe(1)–N(3)	83.4(1)	O(3)–Fe(2)–N(6)	100.7(1)
O(5)–Fe(1)–N(1)	92.9(1)	O(4)–Fe(2)–N(4)	175.1(1)
O(5)–Fe(1)–N(2)	165.1(1)	O(4)–Fe(2)–N(5)	96.7(1)
O(5)–Fe(1)–N(3)	93.2(1)	O(4)–Fe(2)–N(6)	83.8(1)
N(1)–Fe(1)–N(2)	78.4(1)	N(4)–Fe(2)–N(5)	79.1(1)
N(1)–Fe(1)–N(3)	93.9(1)	N(4)–Fe(2)–N(6)	97.7(1)
N(2)–Fe(1)–N(3)	75.5(1)	N(5)–Fe(2)–N(6)	76.9(1)
Fe(1)–O(1)–Fe(2)	115.1(1)		

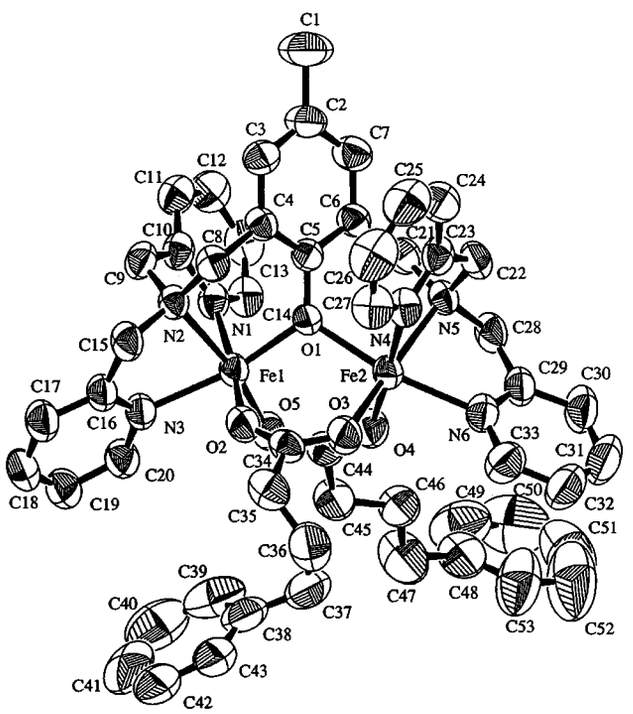

Fig. 12 Crystal structure of $[Fe_2(bpmp)(pba)_2]^{2+}$ in complex **4** at 293 K with 50% probability of thermal ellipsoids.

transition of the counter ions from order to disorder seems not to be a factor affecting the electron transfer rates in these dinuclear bpmp complexes.

If there is a symmetry axis in the middle of the two iron atoms such as in complex **7** the potential-energy surface for the ground state is symmetrized, and the energies of the two vibronic states, $Fe_A^{2+}Fe_B^{3+}$ and $Fe_A^{3+}Fe_B^{2+}$, are identical. The appreciable potential-energy barrier to interconversion of the two states becomes smaller, and the intramolecular electron transfer gradually becomes faster with an increase in temperature.

The stability of a conformation of a molecule in the solid would be controlled by intermolecular interactions in the crystal packing. Packing diagrams of complexes **7** and **4** are shown in Figs. 13 and 14, respectively, which indicate the two

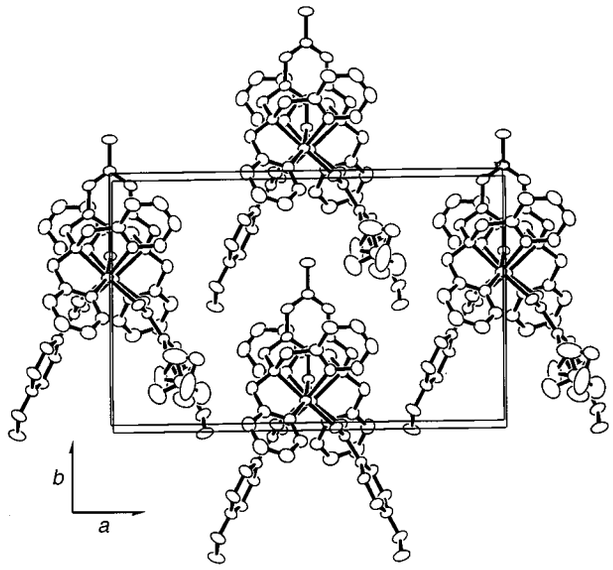

Fig. 13 A projection of the crystal structure of complex **7** at 293 K along the *c* axis.

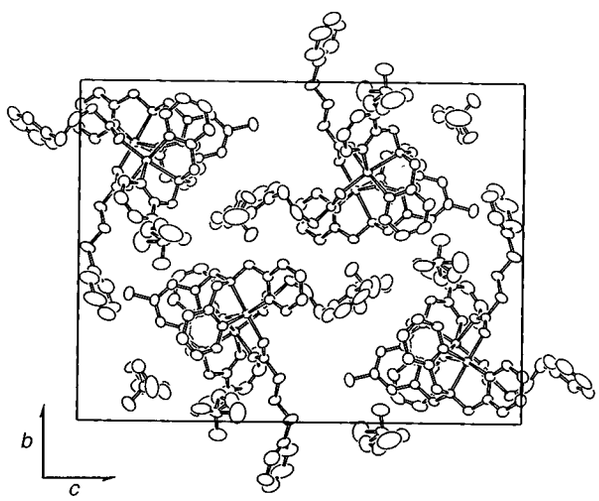

Fig. 14 A projection of the crystal structure of complex **4** at 293 K along the *a* axis.

arrangements are completely different. It is unique that the molecules of **7** are arranged along the *b* axis which is also a C_2 axis. The anions are sited symmetrically with respect to the C_2 axis. Therefore the shape of the space around a carboxyl group in the solid is the same as that around the other carboxyl group. In the case of **4** the two carboxylic acids co-ordinating to a cation are inserted in the spaces formed by the arrangement of the neighboring molecules, and the spaces around the two carboxylic acids are entirely different in shape, which makes the geometry around the cations asymmetric. It is important to point out that the molecule should have C_2 symmetry or close to it to experience rapid intramolecular electron exchange. For molecules having long chain carboxylic acids part of the chains would influence the molecular packing.

The relationship between crystal structures and mixed-valence states has been studied in biferrocene derivatives: 1′, 1″-dibutylbiferrocenium triiodide crystallizes in two different forms, one of which shows a conversion from valence trapped to detrapped in Mössbauer spectra and the other shows trapped spectra at the temperatures from 78 K to room temperature.[34] Two crystallographically distinct iron moieties are observed in both forms and the former are more symmetric than the latter.[35]

X-Ray powder diffraction patterns

The X-ray powder diffraction patterns of the complexes were

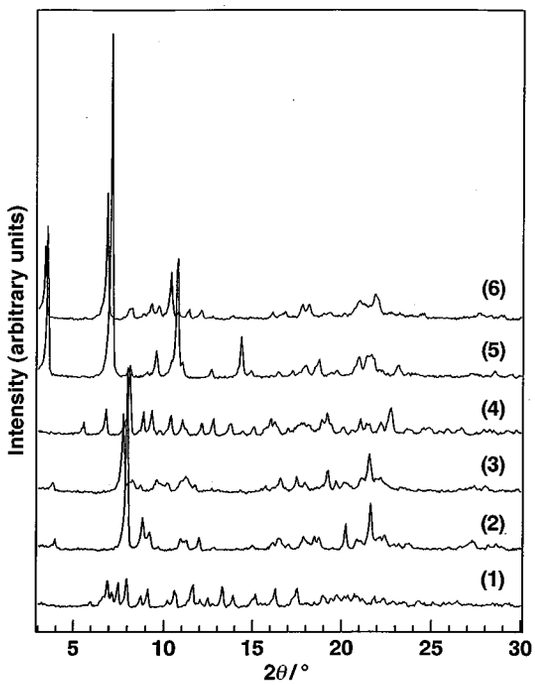

Fig. 15 X-Ray power diffraction patterns for the complexes.

measured at room temperature and are shown in Fig. 15. Although the difference in the chemical structure among the complexes except **7** is just in the lengths of the alkyl chains of the carboxylic acids, the diffraction patterns are different. Those of **5** and **6** are characteristic of layered structures: there are some peaks with equal intervals in the low-angle region. The first, second and third peaks from the lowest diffraction angles are assigned to (010), (020) and (030) planes, respectively, and the length of the *b* axis of **6** is estimated to be 25.8 Å on this basis, comparable to that of $[Fe_2(bpmp)\{CH_3(CH_2)_5CO_2\}_2][BF_4]_2$ (23.5 Å).[13b] The difference between the two values is due to the difference in the length of the terminal groups of the carboxylic acids, *i.e.* methyl and phenyl. The powder patterns of **2** and **3** are similar to each other, and those of **1** and **4** are different from the others. The variation in crystal structure is observed among the complexes with short methylene chains, suggesting that the rearrangement of not only the iron moieties but also the ligands is an important factor in determining the rate of intramolecular electron transfer.

Conclusion

Mixed-valence $Fe^{II}Fe^{III}$ bpmp complexes **5** and **6** with long carboxylate chains show valence detrapped Mössbauer spectra at 293 K and have layer structures. The Mössbauer spectra of **7** convert from valence trapped to detrapped on increasing the temperature. The two iron atoms in the crystal structure of **7** are crystallographically equivalent at 130 and 293 K, indicating the temperature-dependent Mössbauer spectra are attributed to electron exchanges between two vibronic states which are at the same energy levels. Complexes **1**, **2** and **4** with short carboxylate chains show valence-trapped Mössbauer spectra even at 293 K, and there is no crystallographically imposed symmetry for **4** at 293 K. Complex **3** is the first example demonstrating $Fe^{2.2+}$ and $Fe^{2.8+}$ valence states upon Mössbauer spectroscopy. These results suggest that the rate of intramolecular electron transfer is very sensitive to the packing arrangement in the bpmp complexes. Study of the electron transfer in solution would be important to determine the effect of intermolecular interaction on the rate. The sensitivity of the rate to the packing arrangement suggests that the rate could be controlled by change in the molecular structure according to the pressure, temperature, light irradition, *etc.*

Experimental

Syntheses of the complexes

The bpmp complexes were synthesized according to a method reported elsewhere.[10] Single crystals for X-ray analysis were obtained from a 1:1 acetonitrile–ethanol solution {Calc. for $[Fe_2(bpmp)_2][BF_4]_2$ **1** ($C_{47}H_{43}B_2F_8Fe_2N_6O_5$): C, 53.40; H, 4.10; Fe, 10.57; N, 7.95. Found: C, 53.02; H, 4.09; Fe, 10.42; N, 7.91. Calc. for $[Fe_2(bpmp)(paa)_2][BF_4]_2$ **2** ($C_{49}H_{47}B_2F_8Fe_2N_6O_5$): C, 54.23; H, 4.37; Fe, 10.29; N, 7.74. Found: C, 54.38; H, 4.41; Fe, 10.09; N, 7.83. Calc. for $[Fe_2(bpmp)(ppa)_2][BF_4]_2$ **3** ($C_{51}H_{51}B_2F_8Fe_2N_6O_5$): C, 55.02; H, 4.62; Fe, 10.03; N, 7.55. Found: C, 54.52; H, 4.68; Fe, 9.85; N, 7.66. Calc. for $[Fe_2(bpmp)(pba)_2][BF_4]_2$ **4** ($C_{53}H_{55}B_2F_8Fe_2N_6O_5$): C, 55.77; H, 4.86; Fe, 9.79; N, 7.36. Found: C, 55.27; H, 4.89; Fe, 9.75; N, 7.37. Calc. for $[Fe_2(bpmp)(pva)_2][BF_4]_2$ **5** ($C_{55}H_{59}B_2F_8Fe_2N_6O_5$): C, 56.49; H, 5.09; Fe, 9.55; N, 7.19. Found: C, 55.96; H, 5.01; Fe, 9.38; N, 7.15. Calc. for $[Fe_2(bpmp)(pha)_2][BF_4]_2$ **6** ($C_{57}H_{63}B_2F_8Fe_2N_6O_5$): C, 57.17; H, 5.14; Fe, 9.33; N, 7.02. Found: C, 56.56; H, 5.16; Fe, 9.28; N, 6.96. Calc. for $[Fe_2(bpmp)(mba)_2][BF_4]_2$ **7** ($C_{49}H_{47}B_2F_8Fe_2N_6O_7$): C, 52.68; H, 4.24; Fe, 10.00; N, 7.52. Found: C, 52.18; H, 4.25; Fe, 9.94; N, 7.44%}.

Physical measurements

Microanalysis for carbon, hydrogen, and nitrogen was carried out at the Elemental Analysis Center, Kyushu University. Quantitative analysis for iron was performed by atomic absorption analysis, using an Atomic Absorption/Flame Emission Spectrometer AA-625-11 (Shimadzu). Absorption and reflectance spectra were measured using a Shimazu UV-3100PC self-recording spectrophotometer from 300 to 2000 nm.

Cyclic voltammetry of the complexes in acetonitrile (containing 0.1 M Bu_4NClO_4 as supporting electrolyte) were carried out on an AC/DC Cyclic Polarograph P-900 (Yanaco) at 293 K under an argon atmosphere. A standard three-electrode system comprising a glassy carbon working electrode, a saturated Ag–AgCl (RE-5, BAS) reference electrode and a platinum counter electrode was employed. Ferrocene was used as a standard substance. The observed values for the complexes were converted into redox potentials *versus* SCE by using the eqn. (13).

$$\text{Redox potential for the complex} = \text{observed value for a complex} - \text{observed value for ferrocene} + 0.0739 \text{ (ferrocene } \textit{vs.} \text{ Ag–AgCl)}^{36} + 0.272 \text{ (SCE } \textit{vs.} \text{ Ag–AgCl)}^{36} \quad (13)$$

Mössbauer spectra were measured with an S-600 constant-acceleration spectrometer (Austin Science Associates). Temperature was controlled with a type ITC502 (Oxford Instruments) controller within a variable temperature cryostat, type DN1726 (Oxford Instruments). The data were stored in a 1024-channel analyzer, type IT-5200 (Inotech Inc.). A 10 mCi ^{57}Co source diffused into palladium foil was used. The spectra were fitted by a Lorentzian line shape by using software of IGOR Pro (WaveMetrics, Inc.) on a personal computer, and the velocity scales and isomer shifts were normalized to iron foil at room temperature. The X-ray powder diffraction patterns were recorded with Cu-Kα X-rays on a Model XD-D1 (Shimadzu) diffractometer.

Crystal structure determinations

Complex 4 at 293 K. Intensity data were obtained from a dark green crystal (0.4 × 0.2 × 0.2 mm) placed on a Rigaku AFC7R four-circle diffractometer. Graphite monochromatized Mo-Kα radiation ($\lambda = 0.71069$ Å) was used. For the intensity collections the $\bar{\omega}$–2θ scan mode was used to a maximum 2θ value of 50.1° min^{-1}. Of the 10460 relfections collected, 9894 were unique, and no significant decline in intensities of three

Table 6 Crystallographic data for complexes **7** and **4**

	7		**4**
Formula	$C_{49}H_{47}B_2F_8Fe_2N_6O_7$		$C_{53}H_{55}B_2F_8Fe_2N_6O_5$
M	1117.25		1141.36
T/K	130	293	293
Crystal system	Monoclinic	Monoclinic	Monoclinic
Space group	$C\,2/c$	$C\,2/c$	$P2_1/c$
a/Å	20.672(6)	20.990(5)	10.701(6)
b/Å	12.204(4)	12.194(3)	19.725(3)
c/Å	22.487(4)	23.003(3)	25.737(4)
β/°	113.24(2)	114.12(1)	93.43(3)
U/Å^3	5212(2)	5373(1)	5422(2)
Z	4	4	4
D/g cm^{-3}	1.42	1.38	1.40
D_m/g cm^{-3}		1.37	1.39
μ/cm^{-1}	6.40	6.20	6.14
R	0.055	0.047	0.042
R'	0.054	0.046	0.052

standard reflections was observed. The data were corrected for Lorentz-polarization effects. Crystallographic data are summarized in Table 6. The structures were solved by the direct method and Fourier techniques, and refined by full-matrix least squares. Neutral atom scattering factors were taken from Cromer and Waber.[37] Anomalous dispersion effects were included in F_c;[38] the values for $\Delta f'$ and $\Delta f''$ were those of Creagh and McAuley.[39] The values for the mass attenuation coefficient are those of Creagh and Hubbell.[40] All calculations were performed using the TEXSAN[41] crystallographic software package. The final cycle of full-matrix least-squares refinement was based on 6823 observed reflections [$I > 3\sigma(I)$].

Complex 7 at 293 and 130 K. A dark green single crystal (0.3 × 0.3 × 0.1 mm) of complex **7** was mounted on a Rigaku 7S four-circle diffractometer equipped with a liquid N_2 cryostream cooler (Oxford Cryosystems). The number of measured reflections was 6647, with 6470 unique at 293 K, and 6420, with 6248 unique at 130 K, respectively. No decay in intensity was observed during the measurements. Crystallographic data are collected in Table 6. The structures were solved and refined as for **4**. All non-hydrogen atoms were readily located and refined with anisotropic thermal parameters. Hydrogen atoms were located from the structure-factor calculations. At both temperatures a C_2 axis is present along C(1)–C(2)–C(5)–O(1) and calculated hydrogen atoms of C(1) lie just off the axis. Therefore three hydrogen atoms, the populations of which are 0.5, were placed on C(1) before applying a symmetry expansion. The final refinements were carried out with 2456 unique reflections [$I > 3\sigma(I)$] and with 2580 at 130 K.

CCDC reference number 186/1339.

See http://www.rsc.org/suppdata/dt/1999/1001/ for crystallographic files in .cif format.

Acknowledgements

We thank Yukari Shima of Kurume Institute of Technology for her kind measurements of the spectra. This work was supported by Yoshida Society of the Promotion of Science and Education, and a Grant-in-Aid for Scientific Research No. 06453052 from the Ministry of Education, Science and Culture, which are greatly acknowledged.

References

1 R. E. Stenkamp, L. C. Sieker, L. H. Jensen and J. Sanders-Loehr, *Nature* (*London*), 1981, **291**, 263; R. E. Stenkamp, L. C. Sieker and L. H. Jensen, *J. Am. Chem. Soc.*, 1984, **106**, 618.
2 P. C. Wilkins and R. G. Wilkins, *Coord. Chem. Rev.*, 1987, **79**, 195; R. G. Wilkins and P. C. Harrington, *Adv. Inorg. Biochem.*, 1983, **5**, 51.
3 L. Yhelander and P. Reichard, *Annu. Rev. Biochem.*, 1979, **48**, 133; P. Reichard and A. Ehrenberg, *Science*, 1987, **221**, 514; B. M. Sjöberg, T. M. Loehr and J. Sanders-Loehr, Jr., *J. Biochem.*, 1982, **21**, 96.
4 J. G. Dewitt, J. G. Bensten, A. C. Rosenzweig, B. Hedman, J. Green, S. Pilkington, G. C. Bensten, G. C. Papaefthymiou, H. Dalton, K. O. Hodgson and S. J. Lippard, *J. Am. Chem. Soc.*, 1991, **113**, 9219.
5 B. G. Fox,W. A. Froland, J. E. Dege and J. D. Lipsscomb, *J. Biol. Chem.*, 1989, **264**, 10023.
6 M. P. Woodland and H. Dalton, *J. Biol. Chem.*, 1984, **259**, 53.
7 B. A. Averill, J. G. Davis, S. Burman, T. Zirino, J. Sanders-Loehr, T. M. Loehr, J. T. Sage and P. G. Debrunner, *J. Am. Chem. Soc.*, 1987, **109**, 3760; S. M. Kauzlarich, B. K. Teo, T. Zirino, S. Burman, J. C. Davis and B. A. Averill, *Inorg. Chem.*, 1986, **25**, 2781.
8 E. Sinn, G. J. O'Connor, J. de Jersey and B. Zerner, *Inorg. Chim. Acta,*, 1983, **78**, L13.
9 B. C. Antanaitis and P. Aisen, *Adv. Inorg. Biochem.*, 1983, **5**, 111.
10 M. Suzuki, A. Uehara, H. Oshio, K. Endo, M. Yanagi, S. Kida and K. Saito, *Bull. Chem. Soc. Jpn.*, 1987, **60**, 3547; 1988, **61**, 3907.
11 (*a*) A. S. Borovik, B. P. Murch and L. Que, Jr., *J. Am. Chem. Soc.*, 1987, **109**, 7190; (*b*) M. S. Mashuta, R. J. Webb, K. J. Oberhausen, J. F. Richardson, R. M. Buchanan and D. N. Hendrickson, *J. Am. Chem. Soc.*, 1989, **111**, 2745; (*c*) M. S. Mashuta, R. J. Webb, J. K. McCusker, E. A. Schmitt, K. J. Oberhausen, J. F. Richardson, R. M. Buchanan and D. N. Hendrickson, *J. Am. Chem. Soc.*, 1992, **114**, 3815; (*d*) A. S. Borovik and L. Que, Jr., *J. Am. Chem. Soc.*, 1988, **110**, 2345.
12 A. Neves, M. A. de Brito, I. Vencato, V. Drago, K. Griesar and W. Haase, *Inorg. Chem.* 1996, **35**, 2360; C. Belle, I. Gautier-Luneau, Jean-Louis Pierre and C. Scheer, *Inorg. Chem.*, 1996, **35**, 3706.
13 (*a*) Y. Maeda, Y. Tanigawa, S. Hayami and Y. Takashima, *Chem. Lett.*, **1992**, 591; (*b*) Y. Maeda, Y. Tanigawa, N. Matsumoto, H. Oshio, M. Suzuki and Y. Takashima, *Bull. Chem. Soc. Jpn.*, 1994, **67**, 125; (*c*) Y. Maeda, Y. Tanigawa, Y. Ando, Y. Takashima and N. Matsumoto, *Acta Chim. Hung.*, *Models in Chem.*, 1993, **130**, 55.
14 S. Nakashima, Y. Ueki and H. Sakai, *J. Chem. Soc.*, *Dalton Trans.*, 1995, 513.
15 T. Nakamoto, M. Katada and H. Sano, *Chem. Lett.*, 1990, 225; 1991, 1323.
16 (*a*) D. N. Hendrickson, in *Applications in Chemistry*, *Physics and Biology*; NATO ASI Series C: Mathematical and Physical Sciences 343, ed. K. Prassides, Kluwer, Dordrecht, 1991, pp. 67–90; (*b*) R. J. Webb, A. L. Rheingold, S. J. Geib, D. L. Staley and D. N. Hendrickson, *Angew. Chem.*, *Int. Ed. Engl.*, 1989, **28**, 1388; (*c*) D. N. Hendrickson, S. M. Oh, T.-Y Dong, T. Kambara, M. J. Cohn and M. F. Moore, *Comments Inorg. Chem.*, 1985, **4**, 329; (*d*) M. Sorai and D. N. Hendrickson, *Pure Appl. Chem.*, 1991, **63**, 1503; (*e*) R. J. Webb, S. J. Geib, D. L. Staley, A. L. Rheingold and D. N. Hendrickson, *J. Am. Chem. Soc.*, 1990, **112**, 5031; (*f*) C.-C. Wu, H. G. Jang, A. L. Rheingold, P. Gütlich and D. N. Hendrickson, *Inorg. Chem.*, 1996, **35**, 4137.
17 H. Sano, *Hyperfine Interact.*, 1990, **53**, 97; S. Nakashima, A. Nishimori, Y. Masuda, H. Sano and M. Sorai, *J. Phys. Chem. Solids.*, 1991, **52**, 1169; K. Asamaki, T. Nakamoto, S. Kawata, H. Sano, M. Katada and K. Endo, *Inorg. Chim. Acta*, 1995, **236**, 155.
18 L. O. Spreer, A. Li, D. B. MacQueen, C. B. Allan, J. W. Otvos, M. Calvin, R. B. Frankel and G. C. Papaefthymiou, *Inorg. Chem.*, 1994, **33**, 1753.
19 Y. Maeda, K. Kawano and T. Oniki, *J. Chem. Soc.*, *Dalton Trans.*, 1995, 3533.
20 G. Williams, G. R. Moore and R. J. P. Williams, *Comments Inorg. Chem.*, 1985, **4**, 55.
21 N. S. Hush, M. N. Paddon-Row, E. Cotsaris, H. Oevering, J. W. Verhoeven and M. Heppener, *Chem. Phys. Lett.*, 1985, **117**, 8.
22 T. Kambara and N. Sasaki, *J. Phys. Soc. Jpn.*, 1982, **51**, 1694.
23 S. H. Adachi, A. E. Panson and R. M. Stratt, *J. Chem. Phys.*, 1988, **88**, 1134.
24 K. Y. Wong, P. N. Schatz and S. B. Piepho, *J. Am. Chem. Soc.*, 1979, **101**, 2793.
25 R. Ingalls, F. V. Woude and G. A. Sawatzky, *Mössbauer Isomer Shift*, eds. G. K. Shenoy and F. E. Wagner, North-Holland, Amsterdam, 1978, (*a*) p. 101, (*b*) p. 361.
26 *Mössbauer Spectroscopy and Transition Metal Chemistry*, eds. P. Gütlich, R. Link and A. Trautwein, Springer, Berlin, 1978, pp. 69–75.
27 L. R. Walker, G. K. Wertheim and V. Jaccarino, *Phys. Rev. Lett.*, 1961, **6**, 98.
28 R. E. Watson, *Phys. Rev.*, 1960, **119**, 1934.
29 H. H. Wickman, *Mössbauer Effect Methodology*, ed. I. J. Gruverman, Plenum, New York, 1966, pp. 39–66.
30 Y. Masuda and H. Sano, *Bull. Chem. Soc. Jpn.*, 1987, **60**, 2674.

31 S. Iijima, I. Motoyama and H. Sano, *Bull. Chem. Soc. Jpn.*, 1980, **53**, 3180.
32 T. Sato, F. Ambe, K. Endo, M. Katada, H. Maeda, T. Nakamoto and H. Sano, *J. Am. Chem. Soc.*, 1996, **118**, 3450.
33 H. G. Jang, K. Kaji, M. Sorai, R. J. Witterbrot, S. J. Geib, A. L. Rheingold and D. N. Hendrickson, *Inorg. Chem.*, 1990, **29**, 3547; H. G. Jang, S. J. Geib, Y. Kaneko, M. Nakano, M. Sorai, A. L. Rheingold, B. Montez and D. N. Hendrickson, *J. Am. Chem. Soc.*, 1989, **111**, 173; Y. Kaneko, M. Nakano, M. Sorai, H. G. Jang and D. N. Hendrickson, *Inorg. Chem.*, 1989, **28**, 1067; H. G. Jang, R. J. Witterbrot, M. Sorai, Y. Kaneko, M. Nakano and D. N. Hendrickson, *Inorg. Chem.*, 1992, **31**, 2265.
34 S. Nakashima, Y. Masuda, I. Motoyama and H. Sano, *Bull. Chem. Soc. Jpn.*, 1987, **60**, 1673.
35 S. Nakashima, M. Konno and H. Sano, *Hyperfine Interact.*, 1991, **68**, 205.
36 *Kagakubinran*, *Kisohen II*, Nippon Kagakukai, Maruzen, Tokyo, 1975, p. 1207.
37 D. T. Cromer and J. T. Waber, *International Tables for X-Ray Crystallography*, Kynoch Press, Birmingham, 1974, vol. IV, Table 2.2A.
38 J. A. Ibers and W. C. Hamilton, *Acta Crystallogr.*, 1964, **17**, 781.
39 D. C. Creagh and W. J. McAuley, *International Tables for Crystallography*, ed. A. J. C. Wilson, Kluwer, Boston, 1992, vol. C, Table 4.2.6.8, pp. 219–222.
40 D. C. Creagh and J. H. Hubbell, *International Tables for Crystallography*, Kluwer, Boston, 1992, Vol. C, Table 4.2.4.3, pp. 196–206.
41 TEXSAN, Crystal Structure Analysis Package, Molecular Structure Corporation, Houston, TX, 1985 and 1992.

Paper 8/08069K